

UC Riverside

2016 Publications

Title

Using a new inversion matrix for a fast-sizing spectrometer and a photo-acoustic instrument to determine suspended particulate mass over a transient cycle for light-duty vehicles

Permalink

<https://escholarship.org/uc/item/9zv7t3dx>

Journal

Aerosol Science and Technology, 50(11)

ISSN

0278-6826 1521-7388

Authors

Xue, Jian
Li, Yang
Quiros, David
et al.

Publication Date

2016-09-22

DOI

10.1080/02786826.2016.1239247

Peer reviewed




Using a new inversion matrix for a fast-sizing spectrometer and a photo-acoustic instrument to determine suspended particulate mass over a transient cycle for light-duty vehicles

Jian Xue, Yang Li, David Quiros, Xiaoliang Wang, Thomas D. Durbin, Kent C. Johnson, Georgios Karavalakis, Shaohua Hu, Tao Huai, Alberto Ayala & Heejung S. Jung


To cite this article: Jian Xue, Yang Li, David Quiros, Xiaoliang Wang, Thomas D. Durbin, Kent C. Johnson, Georgios Karavalakis, Shaohua Hu, Tao Huai, Alberto Ayala & Heejung S. Jung (2016) Using a new inversion matrix for a fast-sizing spectrometer and a photo-acoustic instrument to determine suspended particulate mass over a transient cycle for light-duty vehicles, *Aerosol Science and Technology*, 50:11, 1227-1238, DOI: [10.1080/02786826.2016.1239247](https://doi.org/10.1080/02786826.2016.1239247)

To link to this article: <https://doi.org/10.1080/02786826.2016.1239247>


 View supplementary material 

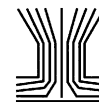
 Accepted author version posted online: 22 Sep 2016.
Published online: 11 Oct 2016.

 Submit your article to this journal 

 Article views: 331

 View Crossmark data 

 Citing articles: 4 View citing articles 



Using a new inversion matrix for a fast-sizing spectrometer and a photo-acoustic instrument to determine suspended particulate mass over a transient cycle for light-duty vehicles

Jian Xue^{a,b}, Yang Li^{a,b}, David Quiros^c, Xiaoliang Wang^d, Thomas D. Durbin^a, Kent C. Johnson^a, Georgios Karavalakis^a, Shaohua Hu^c, Tao Huai^c, Alberto Ayala^c, and Heejung S. Jung^{a,b}

^aCenter for Environmental Research and Technology, Bourns College of Engineering, University of California—Riverside, Riverside, California, USA; ^bDepartment of Mechanical Engineering, University of California—Riverside, Riverside, California, USA; ^cCalifornia Air Resources Board (CARB), Sacramento, California, USA; ^dDesert Research Institute, Reno, Nevada, USA

ABSTRACT

Integrated particle size distribution (IPSD) is a promising alternative method for estimating particulate matter (PM) emissions at low levels. However, a recent light-duty vehicle (LDV) emissions study showed that particle mass estimated using IPSD (M_{IPSD}) with the TSI Engine Exhaust Particle Sizer (EEPS) Default Matrix was 56–75% lower than mass derived using the reference gravimetric method (M_{Grav}) over the Federal Test Procedure (FTP). In this study, M_{IPSD} calculated with a new inversion matrix, the Soot Matrix, is compared with M_{Grav} and also photoacoustic soot mass (M_{Soot}), to evaluate potential improvement of the IPSD method for estimating PM mass emissions from LDVs. In addition, an aerodynamic particle sizer (APS) was used to estimate mass emission rates attributed to larger particles (0.54–2.5 μm in aerodynamic diameter) that are not measured by the EEPS. Based on testing of 10 light-duty vehicles over the FTP cycle, the Soot Matrix significantly improved agreement between M_{IPSD} and M_{Grav} by increasing slopes of M_{IPSD}/M_{Grav} from 0.45–0.57 to 0.76–1.01 for gasoline direct injected (GDI) vehicles; however, for port-fuel injection (PFI) gasoline vehicles, a significant discrepancy still existed between M_{IPSD} and M_{Grav} , with M_{IPSD} accounting for $34 \pm 37\%$ of M_{Grav} . For all vehicles, strong correlations between M_{IPSD} and M_{Soot} were obtained, indicating the IPSD method is capable of capturing mass of soot particles. The discrepancy between the M_{IPSD} and M_{Grav} for PFI vehicles, which have relatively low PM emissions (0.22 to 1.83 mg/mile), could be partially due to limited size range of the EEPS by not capturing larger particles (0.54–2.5 μm) that accounts for ~ 0.08 mg/mile of PM emission, uncertainties of particle effective density, and/or gas-phase adsorption onto filters that is not detected by *in situ* aerosol instrumentation.

ARTICLE HISTORY

Received 18 February 2016
Accepted 28 August 2016

EDITOR

Jian Wang

1. Introduction

There is a growing interest in determining vehicle particulate emissions using *in situ* real time aerosol instruments due to their potential advantages such as high temporal resolution, sensitivity, cost-effective, and minimal artifact interference. Maricq et al. (2016) evaluated ability of three aerosol instruments (Dekati Mass Monitor, Engine Exhaust Particle Spectrometer, and Micro Soot Sensor) to measure regulatory metrics such as $\text{PM}_{2.5}$ mass for the U.S. regulation and solid particle number (SPN) for E.U. regulation, Mohr et al. (2005) evaluated 16 different particle measurement systems to measure both regulatory (PM mass and SPN) and non-regulatory metrics (black carbon (BC), particle surface area, PN, etc.). BC mass from light-duty vehicles are of

current interest due to its implication to climate change and traffic-related emissions, and it was determined by Bahreini et al. (2015) and Kamboures et al. (2013) in addition to gravimetric method.

The Integrated Particle Size Distribution (IPSD) method is a promising alternative for measuring particulate matter (PM) emissions at low emission levels (Maricq and Xu 2004; Liu et al. 2009; Giechaskiel et al. 2012; Xue et al. 2015). This method determines real-time particulate mass by multiplying the particle volume concentration derived from the particle size distribution and size-dependent particle effective densities. Additionally, real-time IPSD data help better understand the transient nature of emissions, such as during cold-start events. The IPSD method was initially conceptualized by Maricq

CONTACT Heejung S. Jung heejung@engr.ucr.edu Department of Mechanical Engineering, University of California—Riverside, A357 Bourns Hall, 900 University Ave., Riverside, CA 92521, USA.

Color versions of one or more of the figures in the article can be found online at www.tandfonline.com/uast.

Supplemental data for this article can be accessed on the publisher's website.

and Xu (2004) and further evaluated by Liu et al. (2009). Liu et al. (2009) showed that mass obtained using IPSD were within 10 to 20% of gravimetric PM for heavy-duty diesel engines using the Engine Exhaust Particle Sizer (EEPS, TSI Inc., Shoreview, MN, USA). However, we found more recently that M_{IPSD} mass was persistently lower than the gravimetric mass by 37–75% over Federal Test Procedure (FTP) tests for a large dataset of more than 182 tests from 40 light-duty vehicles when using the same EEPS model (Li et al. 2014; Quiros et al. 2015b).

To better understand the discrepancy between M_{IPSD} and M_{Grav} , Quiros et al. (2015a) and Xue et al. (2015) evaluated the accuracy of size distributions measured by the EEPS relative to scanning mobility particle sizer (SMPS) reference measurements under steady-state conditions. The Default inversion matrix used by the EEPS underestimated particles with mobility diameter larger than 100 nm, which generally contributes notably to the total PM mass. Quiros et al. (2015a) derived and applied an *ad hoc* correction to the EEPS data based on SMPS measurements, which increased M_{IPSD} by approximately 14%, which was insufficient to resolve the observed underestimation. When adding the mass contribution of larger particles between 0.54 and 2.5 μm in aerodynamic diameter measured by the Aerodynamic Particle Sizer (APS, TSI Inc., Shoreview, MN, USA), the corrected EEPS and APS data virtually eliminated the bias between M_{IPSD} and M_{Grav} . Similar size underestimations for soot particles were observed with the Cambustion DMS500 Fast Particle Analyzer (Cambustion Ltd., Cambridge, UK), which measures particle size distributions with the same principle as the EEPS (Symonds et al. 2007). Calibration with soot particles and lognormal fitting to the size distributions were employed to improve the DMS number and mass concentration agreement with reference instruments (Combustion 2007; Symonds and Reavell 2007). A fundamental study conducted by Wang et al. (2016a,b) demonstrated that the EEPS Default Matrix was deficient in its ability to measure accurate size distributions of vehicle exhaust particles, especially those with substantial carbonaceous aggregates, which tend to acquire more charge during the unipolar diffusion charging process. To address this shortcoming, the authors conducted additional measurements to characterize the charge distribution of particles with varying morphologies, and improve the accuracy of the EEPS inversion matrix (Wang et al. 2016a,b). Using these measurements, TSI recently developed and released a new matrix, the Soot Matrix (TSI 2015; Wang et al. 2016b), for measuring vehicle exhaust particles. We recently demonstrated that application of the Soot Matrix improves the accuracy of EEPS size distributions substantially for four types of vehicles under steady-state

conditions, and increases M_{IPSD} by 33–53% compared to the baseline determined by the Default Matrix (Xue et al. 2015).

Although the Soot Matrix has been demonstrated to improve the accuracy of particle size distributions from vehicle exhaust, the evaluation conducted by Xue et al. (2015) was under steady-state conditions and had no comparison to gravimetric reference measurements. In this study, we evaluate improvements to the IPSD method over transient certification test cycles using the Soot Matrix, and compare mass estimates to gravimetric filter measurements. Ten light-duty vehicles were tested for this study, including six gasoline direct injection (GDI) vehicles, three port fuel injection (PFI) vehicles, and one light-duty diesel vehicle (LDD) equipped with a diesel particulate filter (DPF). To further explore the nature of PM mass determined by different methods, we also compared M_{IPSD} with the soot particle mass determined by the AVL Micro Soot Sensor (MSS) (M_{Soot}). Additionally, an Aerodynamic Particle Sizer (APS) was used during three tests to quantify the contribution of PM mass from larger particles (0.54–2.5 μm in aerodynamic diameter) during transient operation.

2. Experimental

2.1. Instrumentation and laboratory setup

Testing was conducted at two labs, the Vehicle Emissions Research Laboratory (VERL) at the Bourns College of Engineering-Center for Environmental Research and Technology (CE-CERT) at the University of California at Riverside, and at the ARB Haagen-Smit Laboratory (HSL) in El Monte, California. Both facilities are equipped with a 48-inch single-roll electric dynamometer for testing light-duty vehicles.

The same model and individual unit of a TSI EEPS (Model 3090, firmware version 3.11, manufactured by TSI Inc.) was used to measure particle size distributions at both laboratories, and a Micro Soot Sensor (MSS, model 483 manufactured by AVL Inc., Graz, Austria) was used to measure soot concentrations at VERL. Because the size measurement range of the EEPS spans from 5.6 to 560 nm, and gravimetric filter measurements are downstream of a cyclone that allows penetration of the particles up to around 2.5 μm , an APS (0.54 to 19.81 μm , model 3321, manufactured by TSI Inc.) was used for tests at HSL to investigate the contribution of PM mass by larger particles (0.54–2.5 μm). At both laboratories, parallel gravimetric filter measurements were conducted for all tests, and real-time instruments (EEPS, MSS, and APS) sampled aerosol without any additional dilution downstream of the CVS. At VERL, real-time

instruments were directly connected to the CVS as shown in Figure 1, whereas at HSL a sampling manifold was used, which included cyclonic removal of PM larger than $\sim 2.5 \mu\text{m}$.

The EEPS uses a unipolar charger to induce a high degree of charge onto particles that are subsequently classified by electrical mobility (Mirme 1994; Biskos et al. 2005). In this study, the measured electrometer currents over 22 electrometers are inverted to particle size distributions into 32 bins using two inversion matrices, known as Default Matrix and Soot Matrix (Xue et al. 2015; Wang et al. 2016a,b). A detailed mathematical description of how the inversion matrix converts electrometer signals to size distributions is given by Wang et al. (2016a). The AVL MSS is based on the photo-acoustic measurement method where the light-absorbing PM components (such as soot particles) are exposed to laser light that is periodically modulated at the acoustical resonant frequency (Schindler et al. 2004). Warming and cooling of particles due to light absorption results in pressure waves that are recorded with a microphone. The instrument is capable of measuring particles up to $10 \mu\text{m}$. The MSS is factory calibrated to a filter-collected PM standard that is composed of at least 95% elemental carbon using a Combustion Aerosol Standard (CAST) burner manufactured by Matter Engineering (Kasper 2009; W. Silvis 2016, personal communication, 9 October 2015; AVL Inc.). The APS determines aerodynamic particle size using a time-of-flight method over two overlapping laser beams (Holm et al. 1997; Peters and Leith 2003). All instruments (EEPS, MSS, and APS) captured transient emissions at 1 Hz or faster.

PM was collected onto 47 mm Whatman Teflon[®]-membrane filters with a pore size of $2 \mu\text{m}$. Figure 1 shows the two laboratory setups that were used to collect filter samples. In setup A, one filter sample was taken

over the entire FTP cycle. The filter face velocity was maintained at 100 cm/s , the maximum allowed by Code of Federal Regulations (CFR) Part 1065 (CFR 2011). Other provisions in CFR Part 1066 (CFR 2012), such as control of filter face temperature to $47 \pm 5^\circ\text{C}$, or flow-weighting were not implemented for setup A. In setup B, one filter was used per phase, and all regulatory and certification guidelines, including sampling temperature control, filter weighting and calculations, followed those described in CFR 1065 and 1066. Both setup A and B were adopted in VERL, while HSL testing was conducted using only setup B (Table 1). A pre-classifier (impactor at VERL and cyclone at HSL) was used upstream of the filter sampling in setup B to eliminate particles with aerodynamic diameters larger than $2.5 \mu\text{m}$. A pre-classifier was not used in setup A. Here, setup A and setup B represent sampling setups without and with CFR Part 1066 requirement implementation, respectively.

Tunnel blanks for filter samples were obtained using the same test protocols, but without vehicle exhaust. The tunnel blanks for filter setup A and filter setup B at VERL were approximately 0.13 ± 0.12 and $0.07 \pm 0.07 \text{ mg/mile}$ (average \pm standard deviation, the same as below), respectively. The tunnel blanks for the filter setup B at HSL was about $0.05 \pm 0.12 \text{ mg/mile}$. US EPA has measured a lower standard deviation which can be converted to an emission rate of $\sim 0.08 \text{ mg/mile}$ under the test condition with filter setup A in VERL (Hu et al. 2014). The relative higher standard deviation measured in VERL is due to that one tunnel blank test had $13 \mu\text{g}$ PM mass collected on the blank filter, while all other tests had PM mass collected lower than $8 \mu\text{g}$. Tunnel blanks for the real time instruments were obtained using their measurements before beginning of each cycle. The tunnel blanks for the MSS was approximately $0.01 \pm 0.04 \text{ mg/mile}$. The tunnel blanks for IPSD using

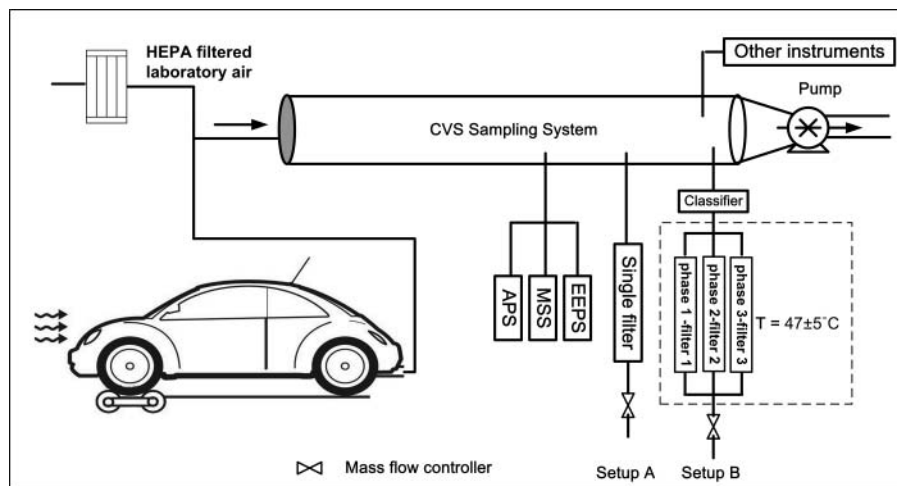


Figure 1. Schematic of laboratory setup at VERL.

Table 1. Summary of the testing specification.

Vehicle ID ^a	Make/Model	Model year	Mileage	Emission category	After-treatment ^b	No. of tests	Test lab	Filter setup
GDI-1	Kia Optima	2012	12K	Tier 2 Bin 5 Cali. LEVII	TWC	1	CE-CERT	A
GDI-2	Mazda 3	2012	19K	Cal. PZEEV	TWC	4	CE-CERT	A
GDI-3	Mercedes Benz	2012	10K	Tier 2 Bin5/ Cal. ULEV II	TWC	2	CE-CERT	A
GDI-4	Ford Escape	2014	25K	US EPA T2B5 LDT2	TWC	2	CE-CERT	B
GDI-5	Ford Focus	2013	31K	Cal. SULFV II	TWC	1	HSL	B
GDI-6	Chevrolet Traverse	2014	14K	Cal. ULEV II	TWC	1	HSL	B
PFI-1	Nissan Versa	2012	2K	Tier 2 Bin5/Cali. ULEV II	TWC	4	CE-CERT	A
PFI-2	Honda Accord	2012	31K	EPA: T2B2 LDV Cali. LEV II SULEV/PZEEV PC	TWC	2	CE-CERT	B
PFI-3	Chevrolet Malibu	2012	27K	ULEV II	TWC	1	HSL	B
LDD	VW Jetta	2009	114K	Cali. ULEV II	DPF LNT	2	CE-CERT	A

^aGDI: Gasoline direct injection; PFI: port fuel injection; LDD: light-duty diesel equipped with a DPF.

^bTWC: Three way catalytic converter; DPF: diesel particle filter; LNT: lean NO₂ trap.

the EEPS were $\leq 0.03 \pm 0.02$ mg/mile at both VERL and HSL, which is likely higher due to the summation of the noise from 22 electrometers of the EEPS rather than from suspended mass within the tunnel. This was confirmed by installing an HEPA filter (TSI. 801625 zero filter) directly onto the inlet of the TSI EEPS, which resulted in a tunnel-blank level of around 0.02 mg/mile for direct HEPA-filtered air.

2.2. Vehicle, fuel, and driving cycle

Ten vehicles were tested in this study, including six GDI vehicles, three PFI vehicles, and one LDD vehicle, selected to provide a variety of different emission levels and engine technologies used in modern vehicles. Detailed specifications of the vehicles are listed in Table 1. At VERL, the vehicles were all tested with either the fuel in the tank at the time it was received (in-use California gasoline) or number 2 diesel fuel purchased from a local gas station (for the LDD vehicle). For the PFI and GDI vehicles tested at HSL, Phase III certification-grade gasoline fuel was used.

The vehicles were tested over the FTP driving cycle, the primary chassis dynamometer certification cycle for light-duty vehicles in the U.S., which consists of three phases. The first phase is the “cold start,” which represents operation when the vehicle is first started following a soak lasting between 8 and 24 h. Phase 2 is the stabilized phase, which represents driving when the engine and aftertreatment system are warmed up. Phase 3 is identical to phase 1, but follows a hot-soak period lasting between 9 and 11 min. The vehicles were preconditioned using the first two FTP phases (the LA-4 preparation cycle) at VERL, and a full three-phase FTP cycle at HSL. No preconditioning was conducted on vehicle PFI-1. A speed time trace for the FTP is presented as Figure S1 in the online supplemental information (SI). Vehicles were tested in this study over the FTP cycle between one and four times (Table 1).

2.3. IPSD method

The IPSD method obtains the PM mass by multiplying the particle volume concentration with the size-dependent particle effective densities, as follows:

$$M_{ipsd} = \sum_i \rho_{eff,i} \cdot \left(\frac{\pi D_{p,i}^3}{6} \right) \cdot n_i, \quad [1]$$

where $D_{p,i}$, n_i , and $\rho_{eff,i}$ are the particle mobility diameter, particle number concentration, and the effective density of the particles in size bin i , respectively.

The effective density varies with particle composition and morphology. We apply effective density according to a power fit model and data measured by Quiros et al. (2015a). Equation (2) shows the particle effective density expressed by mass and mobility scaling exponent (D_m), and a dimensionless constant A derived from experimental data:

$$\rho_{eff} = \frac{AD_p^{D_m-3}}{\pi/6} \quad (D_p \geq 55nm). \quad [2]$$

In this study, we adopt Equation (2) to calculate the particle effective density of particles with mobility diameters equal or larger than 55 nm. For the GDI vehicles, the $D_m = 2.3$ and $A = 9.4$. These values are derived by fitting the data reported in Maricq and Xu (2004) using Equation (2). For the PFI vehicles, the effective density is used according to that reported by Quiros et al. (2015a), where $D_m = 2.67$ and $A = 1.23$. For the LDD vehicle, we adopted values for the GDI vehicles because effective density varies dramatically with the engine operating condition (Quiros et al. 2015a). For particles with mobility diameters between 30 and 55 nm, a constant effective density of particles with D_p of 55 nm was used. A constant effective density of 1.46 g/m³ was applied to particles with mobility diameters equal or smaller than 30 nm, following Zheng et al. (2012). This is the density of hydrated sulfuric acid at room temperature.

The accuracy of the M_{IPSD} depends on the accuracy of the effective density profile adopted. According to Quiros et al. (2015a,b), the particle effective density varied at different steady-state loads. The application of particle effective density achieved at different steady-state loads to the FTP cycle had less than a 1% impact on final mass estimates with the IPSD method. Use of the effective density profile adopted by other researchers (Liu et al. 2009; Quiros et al. 2015a) led to up to a 20% impact on the IPSD mass estimation. The profile of the effective densities applied in this study is shown in Figure S2 in the SI.

3. Results and discussion

3.1. Emission rate of total particle mass and soot

Figure 2 shows PM emission rates determined by the gravimetric method (M_{Grav}), the IPSD method with EEPS Default ($M_{IPSD_Default}$), and Soot Matrix (M_{IPSD_Soot}) for the individual FTP tests for each vehicle. For tests using filter setup B, the PM emission rates were weighted by phase according to typical regulatory measurements of 0.43, 1.00, and 0.57 for phases 1, 2, and 3, respectively (e.g., CRF Part 1066.815(b)) with both

gravimetric filter and real-time measurement methods. However, for the tests with filter setup A, phase weighting was not applied.

PM mass emission rates varied from among vehicles. The GDI vehicles had the highest M_{Grav} , ranging from 0.25 to >6 mg/mile, with GDI-3 having the lowest PM emission rates (<1 mg/mile). The PFI vehicles had lower gravimetric emissions, with M_{Grav} ranging from 0.22 to 1.83 mg/mile. Three of the tests of the PFI-1 had emission rates less than 0.6 mg/mile, while the first test with the PFI-1 had emission rate of ~ 2 mg/mile, which did not include a preconditioning cycle. Note the first data from the PFI-1 shows the importance of preconditioning and included in this article to be consistent with our previous study. However, it was excluded from many forthcoming analyses because no preparation cycle was used. Further studies are needed to fully understand the effect of preconditioning on PM emission from LDVs. PM emission rates obtained without phase weighting (setup A) were typically 20–40% higher than the PM emission rates obtained with phase weighting (setup B). It is because PM emitted during the cold start phase (phase 1) generally dominates the overall PM emission over the FTP cycle and the filter face velocity weighting factor for this phase is only 43% of the nominal with

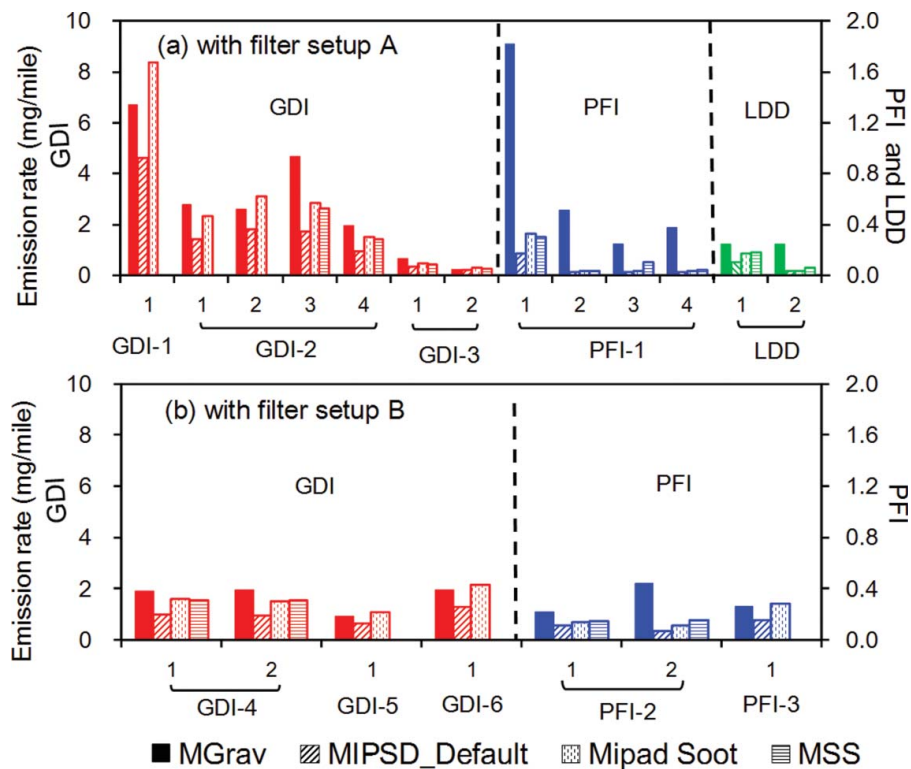


Figure 2. PM emission rate determined by gravimetric method (M_{Grav}), IPSD method with Default ($M_{IPSD_Default}$), and Soot Matrix (M_{IPSD_Soot}), and soot emission rate determined by MSS (M_{soot}) for the individual test with each test vehicle. For tests in (a), the gravimetric method adopted filter setup A. For tests in (b), the gravimetric method adopted filter setup B. Emission rates of the PFI and LDD vehicles were presented on the right y-axis.

setup B. Note, that tests with setup A have been already reported for comparison of gravimetric method and IPSD method using EEPS Default Matrix in Li et al. (2014).

The PM mass emission rates obtained by the IPSD method (M_{IPSD}) also varied among vehicles, which were virtually always lower than paired M_{Grav} values. Most tests and vehicles had M_{IPSD} values below 1 mg/mile, except four GDI vehicles: the GDI-1 that had M_{IPSD} of ~ 8 mg/mile, the GDI-2 that had M_{IPSD} on the order of $\sim 1\text{--}3$ mg/mile, the GDI-4 that had M_{IPSD} of 1–2 mg/mile, and the GDI-6 that had M_{IPSD} of 2 mg/mile. M_{IPSD} values were very low ($<0.1\text{--}0.2$ mg/mile) for all PFI and LDD vehicles, except the first test of PFI-1 that did not undergo the regulatory preparation cycle.

M_{IPSD} shows better agreement with M_{Grav} for all types of vehicles when using EEPS Soot Matrix. On average, M_{IPSD} estimated by EEPS Default Matrix accounted for $57 \pm 13\%$ of the gravimetric mass for the GDI vehicles. When the EEPS Soot Matrix was applied, the M_{IPSD} accounted for $94 \pm 23\%$ of the M_{Grav} for the GDI vehicles.

For the PFI, M_{IPSD} estimated with the Default Matrix accounted for $22 \pm 23\%$ of the M_{Grav} . The estimation of M_{IPSD} was substantially improved to $34 \pm 37\%$ using the Soot Matrix. These improvements are proportional to the improvements achieved for GDI vehicles. This indicates that the Soot Matrix reduced the underestimation of mass using IPSD method for PFI vehicles; however, other uncertainty or limitations appear associated with its equivalency to the gravimetric reference method.

Figure 2 also shows the emission rates of soot particles based on the MSS measurements (M_{Soot}) for the individual test for each tested vehicle. M_{Soot} was constantly lower than M_{Grav} , except the second test with the GDI-3. M_{Soot} accounts for $76 \pm 19\%$ and $29 \pm 22\%$ for the GDI and PFI vehicles, respectively. M_{Soot} accounted for $79 \pm 3\%$ of M_{Grav} by Maricq et al. (2016) in their combined results of GDI and PFI where dominant data were believed to be those by GDI vehicles. These ratios found in the current study appear similar to those calculated between M_{IPSD} and M_{Grav} with the Soot Matrix.

3.2. Cycle-averaged particle size distributions

Figure 3 shows the cycle-averaged size distributions for a test from three selected vehicles (GDI-2, PFI-2, and LDD) for both matrices, and bi-modal lognormal fits to the distributions when Soot Matrix was used. The geometric mean diameter (GMD) and geometric standard deviation (GSD) of the lognormal fits for the nucleation and accumulation modes are listed in Table 2.

For GDI-2, both Default and Soot Matrix resulted in similar GMD for nucleation mode and accumulation mode particles. The GMD for accumulation mode particles (56 nm) was larger than the GMD measured under 60-mph steady-state conditions with a 2% road grade (~ 40 nm) using the same vehicle (Xue et al. 2015). This is likely due to higher emission rate of soot during the cold start phase that could lead to more coagulation or particle growth. The observation is further confirmed when comparing the GMD measured during the cold start and the hot start. During the cold start, the GMDs of accumulation mode particles were 60, 33, and 68 nm for vehicle GDI-2, PFI-2, and LDD, respectively, consistently larger than those during the hot start, which were 44, 22, and 43 nm. In addition, the EEPS Soot Matrix broadened the accumulation size distribution compared to the EEPS Default Matrix (GSD = 1.60 versus 1.93), and increased the concentration of the nucleation mode by 45% at the peak.

For PFI-2, the Default and Soot matrices resulted in a higher fraction of nucleation mode particles compared to GDI-2 (39% versus 27%), indicating PM emitted from PFI vehicles could have a higher composition of semi-volatile constituents (e.g., hydrocarbons and sulfuric acid). The PFI vehicle accumulation mode had a smaller GMD than the GDI vehicle (30 versus 57 nm); this indicates that less and smaller PM was emitted from PFI-2 compared to GDI-2. This may be due to the stratified compared to cleaner-burning premixed flame used by PFI engines. Figure 3b also shows a larger GSD and wider size distribution for the accumulation mode particles when the EEPS Soot Matrix was used (2.31 versus 1.91 with the EEPS Default Matrix). The EEPS Soot Matrix also increased the concentration of nucleation mode particles by approximately 50% compared to the Default Matrix. For the LDD, again, the Soot Matrix lead to broader distributions of the accumulation mode relative to those determined by the Default Matrix (GSD = 2.08 versus 1.79).

3.3. M_{Grav} versus M_{IPSD}

Correlations between M_{Grav} and M_{IPSD} calculated by the Default and Soot Matrix are shown in Figure 4 separated by filter setup and vehicle technology. For GDI vehicle tests, the intercepts of the regression lines were set to be zero in order to better present the ratios between M_{IPSD} and M_{Grav} . Similar regression lines with intercepts are presented in Figure S6 in the SI. The relationship between M_{IPSD} and M_{Grav} has a moderate to strong correlation for the tests with the GDI vehicles, with R^2 varying from 0.53 to

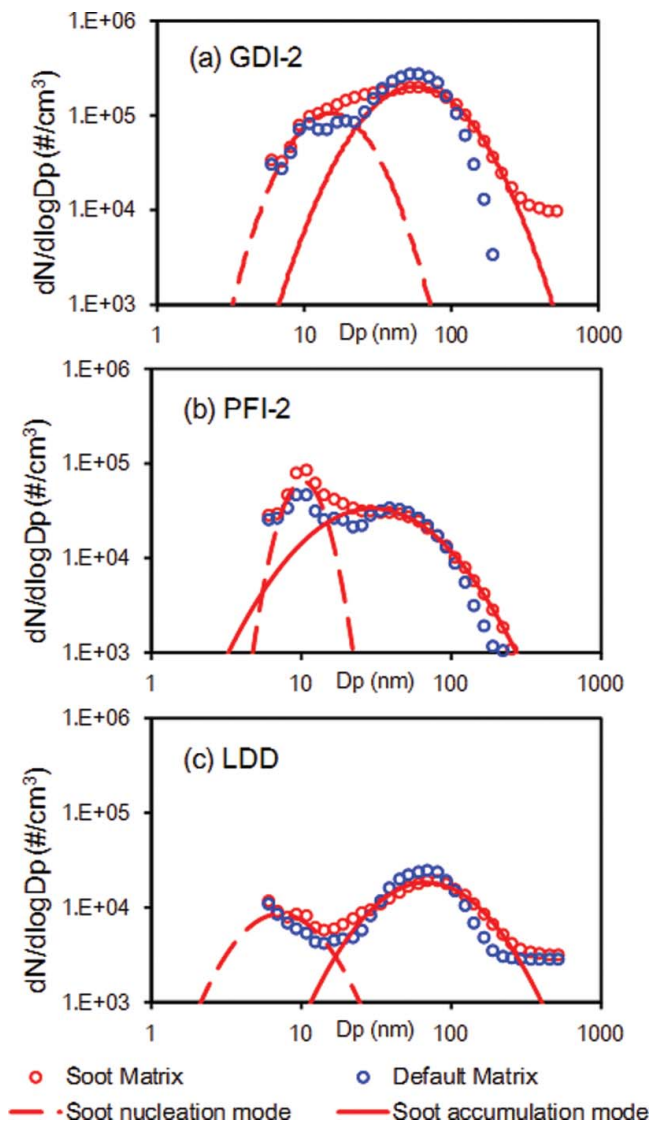


Figure 3. FTP cycle-averaged particle size distributions for vehicle (a) GDI-2, (b) PFI-2, and (c) LDD with EEPS Default and Soot Matrices. Dashed and solid lines present lognormal fitted size distribution of nucleation and accumulation mode particles, respectively, by EEPS Soot Matrix.

0.87. No improvement in the correlation was obtained using the Soot Matrix compared to the Default Matrix; however, the slopes of the best-fit lines when forcing intercepts to zero were much closer to a one-to-one ratio with the Soot Matrix. In the SI, we show stronger correlations ($R^2 = 0.67\text{--}0.90$) when considering non-zero y -intercepts (Figure S6). This result is consistent with that by Maricq et al. (2016).

For GDI vehicles where intercepts are set to zero, the Default Matrix results in slopes of 0.57 and 0.56 for filter setups A and B, respectively. However, the slope for filter setup A is heavily influenced by one data point from GDI-1 that emitted 6.7 mg/mile, which is higher than the relevant limit allowed under any LEV III PM standard. If this test is excluded, the

slope of the test with filter setup A decreased from 0.57 to 0.45, more consistent with earlier findings for light-duty vehicles reported in Quiros et al. (2015b). When the Soot Matrix is applied, the M_{IPSD} agrees much better with M_{Grav} on the tests of the GDI vehicles, and the linear regression slope for M_{IPSD} versus M_{Grav} increases from 0.57 to 1.01 and from 0.45 to 0.76 for the tests with filter setup A, with and without the test on GDI-1, respectively. For tests with filter setup B, the slope for linear regression line increased from 0.56 to 0.92. The subset of tests conducted under filter setup A and B both demonstrate how the Soot Matrix improves results in a closer one-to-one relationship between IPSD and gravimetric mass for GDI vehicles. However, the IPSD method still underestimates gravimetric mass by between 8% or 24% for GDI vehicles, which needs to be further explored.

Correlations between M_{Grav} and M_{IPSD} are negative or absent for the tests for the PFI vehicles as shown in Figures 4b and d. These correlations and figures exclude the first test of PFI-1 because it was not preconditioned using the same test procedures. The lack of positive correlation between M_{Grav} and M_{IPSD} may be due to the uncertainty of the gravimetric method during this test program, variable effective density functions, uncharacteristic size distributions measured during transient operation, or a limited number of tests evaluated. Even when applying the Soot Matrix, the IPSD method systematically underestimates the PM mass for PFI vehicles. Similar correlations were not explored to LDD vehicle due to limited vehicle number of tests.

3.4. M_{IPSD} versus M_{Soot}

The relationship between M_{IPSD} and suspended soot measured by the MSS (M_{Soot}) is compared in Figure 5 to evaluate the soot fraction of suspended particles. Although it is possible to apply phase-weighting to real-time data collected during tests with filter setup A, no adjustment to the real-time data was conducted for consistency with Figures 2 and 4; tests using filter setup B are presented with the flow-weighted emission rate, while tests using filter setup A are presented with flow unweighted emission rates.

Figure 5 shows very strong correlations between M_{Soot} and M_{IPSD} , for both GDI and PFI vehicles, and using either the Soot or Default Matrix. For GDI tests, R^2 is 0.99, notably higher than those fitted for M_{IPSD} and M_{Grav} (0.53–0.87). For PFI tests, R^2 is 0.88 with the Default Matrix and 0.89 with the Soot Matrix. Analysis of the slopes between M_{IPSD} using the Soot Matrix and M_{Soot} using the MSS indicates that the methods are nearly equivalent to within 5%.

Table 2. Parameters for bi-modal fit of FTP cycle from three vehicles.

Test vehicle	Instrument/Matrices	Nucleation mode			Accumulation mode		
		Fraction(%) ^a	GMD(nm) ^b	GSD ^c	Fraction(%)	GMD(nm)	GSD
GDI-2	EEPS Default	25	14	1.77	75	56	1.60
	EEPS Soot	29	15	1.66	71	57	1.93
PFI-2	EEPS Default	39	10	1.39	61	38	1.91
	EEPS Soot	38	10	1.31	62	30	2.31
LDD	EEPS Default	25	7	1.80	75	65	1.79
	EEPS Soot	27	7	1.80	73	69	2.08

^aNumber fraction of particles in this mode; ^bgeometric mean diameters (GMD); ^cgeometric standard deviations (GSD).

Figures 6–8 present real-time and cumulative mass emissions (M_{IPSD} with Soot or Default Matrix, and M_{Soot}) for the selected GDI, PFI, and LDD tests presented in Figure 3, and also show the correlation of 1 Hz data EEPS and MSS data for these tests as a second panel. The three vehicle technologies showed similar PM emission trends (slopes within 10% of a one-to-one ratio using the Soot Matrix) and R^2 values of 0.91, 0.99, and 0.99 are obtained for tests with GDI, PFI, and LDD vehicles, respectively. Additionally, the cumulative emission rates for IPSD using Soot Matrix and M_{Soot} were highly correlated at all points during the FTP cycle. Therefore, the ratio of IPSD to MSS mass is nearly equivalent

even during highly transient operations during the test cycle, and holds true for the GDI, gasoline PFI, and LDD vehicle tests evaluated. These observations could indicate that the IPSD method can capture the solid particles well. It may also indicate that the volatile fraction emitted from these tests was very low. Figures 6–8 reiterate that when using the EEPS Default Matrix, M_{IPSD} is 38%, 57%, and 40% lower than M_{Soot} for the tests on the GDI, PFI, and LDD vehicles, respectively. When applying the newer EEPS Soot Matrix, M_{IPSD} was only 1 and 9% lower than M_{Soot} for the GDI and PFI vehicles, and 1% higher for the LDD vehicle. EEPS measures particles regardless of their chemical composition.

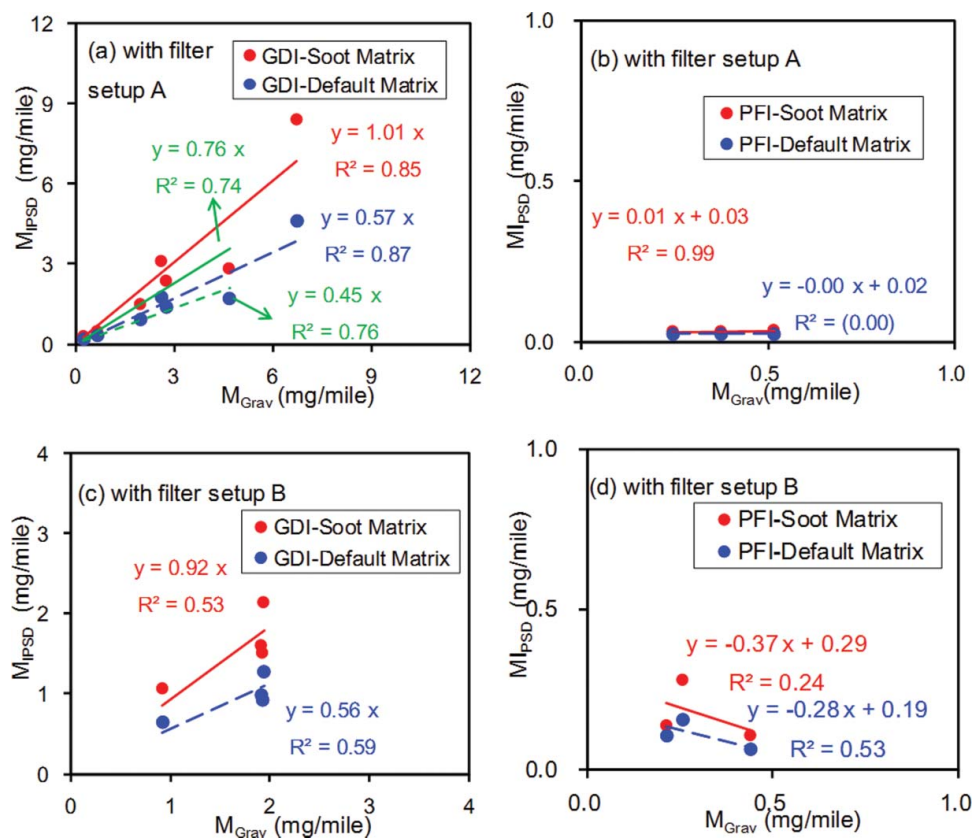


Figure 4. Correlation of PM mass emission rate determined by IPSD method (M_{IPSD}) and gravimetric filter (M_{Grav}): (a) tests with filter setup A for GDI vehicles, (b) tests with filter setup A for PFI vehicles, the first test on PFI-1 is excluded; (c) tests with filter setup B for GDI vehicles; and (d) tests with filter setup B for the PFI vehicles. Two green lines in (a) represent the regression lines excluding the test with vehicle GDI-1, which has an emission rate of 6.7 mg/mile. Regression lines with intercepts are presented in Figure S6 in the SI.

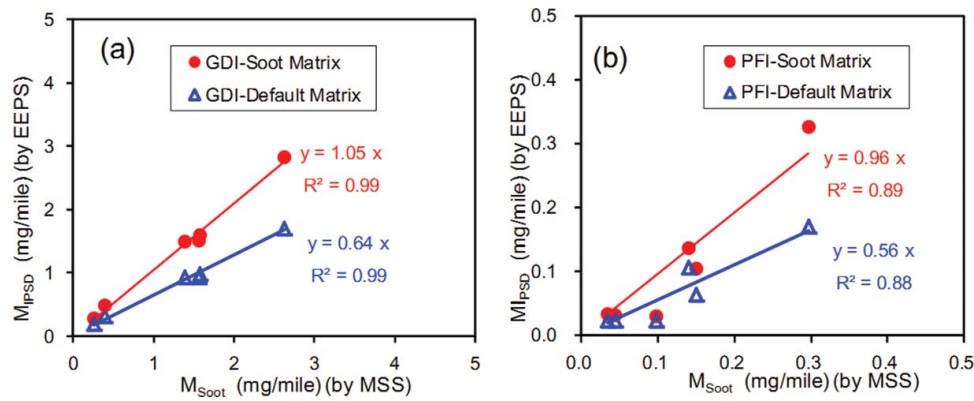


Figure 5. Correlation of PM mass emission rate determined by IPSD method (M_{IPSD}) and micro soot sensor (M_{Soot}) (a) tests with the GDI vehicles, (b) tests with the PFI vehicles. LDD vehicle is not included because of limited test number ($= 2$).

Therefore, the strong one-to-one relationship between M_{IPSD} and M_{Soot} for PFI vehicles indicates that these PFI engines, under these conditions, may have mostly produced EC particles. This is different from the results shown by Fujita et al. (2007) who measured EC/OC composition emitted from PFI vehicles with a quartz filter and showed a predominant OC fraction of PM mass. The regression of 1 Hz data in Figures 6–8 show the correlations between M_{IPSD} and M_{Soot} weaken for data with mass emission rates below $\sim 1 \mu\text{g/s}$. The instrument detection limit of MSS measurement is $10 \mu\text{g/m}^3$. This limit can be translated into the emission rate unit using CVS flow rates to $2.1 \mu\text{g/s}$ for the GDI-2 and LDD, and $0.6 \mu\text{g/s}$ for the PFI-2. The detection limit of M_{IPSD} with the Soot Matrix is $0.2 \mu\text{g/s}$ for the GDI-2 and

LDD, and $0.1 \mu\text{g/s}$ the PFI-2. Therefore, the observed discrepancies between M_{IPSD} and M_{Soot} at low emission levels are likely due to higher detect limit and lower measurement resolution of the MSS. (Note MSS was recently upgraded by the manufacturer to MSSplus, which has $1 \mu\text{g/m}^3$ therefore it may have nearly equal sensitivity compared to the IPSD PM mass determined using EEPS, but this needs to be confirmed by a separate test in the future.)

3.5. PM mass contributed by larger particles

Although it is widely accepted that particles emitted from the vehicles mainly contain nucleation and accumulation mode particles, there is a possibility that a low

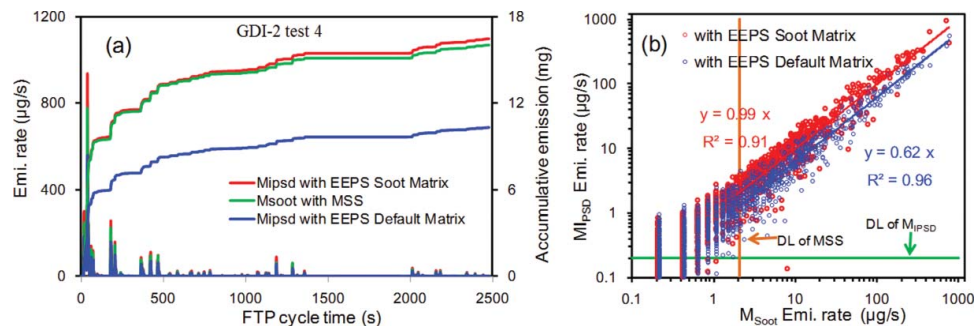


Figure 6. Time series and correlations of M_{IPSD} and M_{Soot} over an FTP cycle of vehicle GDI-2.

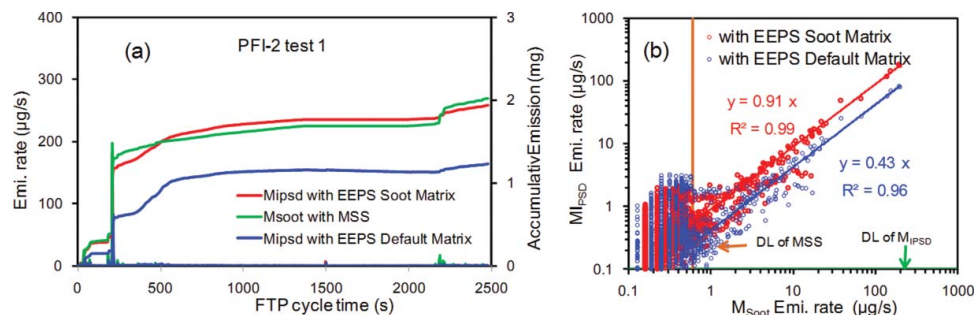


Figure 7. Time series and correlations of M_{IPSD} and M_{Soot} over an FTP cycle of vehicle PFI-2.

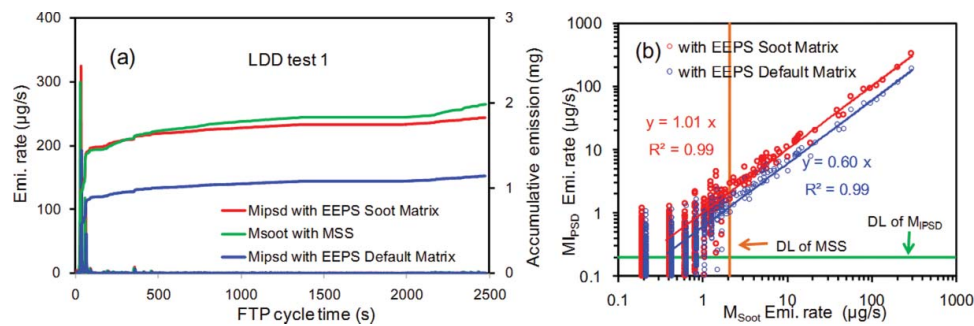


Figure 8. Time series and correlations of M_{IPSD} and M_{Soot} over an FTP cycle of vehicle LDD.

number concentration but significant mass concentration of particles are collected onto filter media that are above mobility diameters larger than measurable using the EEPS (5.6–560 nm). Several previous studies have shown particles that previously deposited on the wall can later re-entrain into the exhaust and form coarse mode particles with mobility diameters typically larger than 1000 nm (Kittelson 1998; Maricq et al. 2011; Quiros et al. 2015a). The coarse mode particles were estimated to contribute 5–20% of the total PM mass for diesel emissions (Kittelson 1998).

Figure 9 compares the M_{IPSD} calculated using the EEPS data (with Soot Matrix) and the APS data. Here, we note lower bound of APS (540 nm in aerodynamic diameter) can be converted to mobility diameter for GDI and PFI vehicles as 1700 and 1240 nm, respectively, assuming power-law fit effective density of 0.12 and 0.22 g/cm³. However, such conversion cannot be made to the upper bound of APS (2.5 µm in aerodynamic diameter), because accumulation mode that is made of soot and so the power-law fit applies does not extend to such large particles.

The results in Figure 9 show the PM mass determined by APS contributed 3.7% and 8.7% of total M_{IPSD} for the

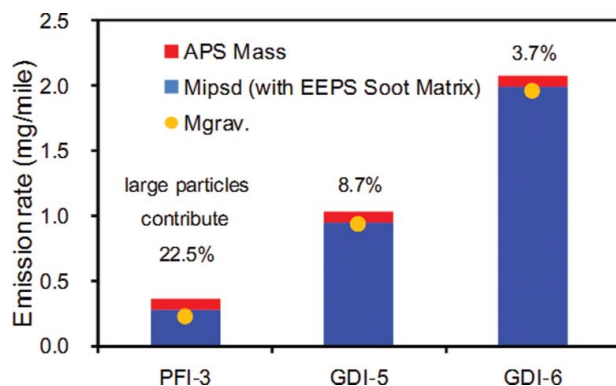


Figure 9. PM emission rate determined by EEPS Soot Matrix, APS, and gravimetric filter during three tests conducted at HSL. The numbers on the accumulative columns represent the percentage of PM mass determined by APS to total PM mass determined by size distribution method (the summing of APS mass and EEPS mass).

tests on the GDI vehicle. This contribution was as high as 22.5% for the test on the PFI vehicle. The contributions by large particles are nearly constant (0.08–0.09 mg/mile) regardless of engine technologies during these three FTP tests. This could suggest that the coarse-mode particles may not be directly emitted from the engine. Additionally, the sum of PM mass estimated from size distributions measured by the EEPS (5.6 to 560 nm in mobility diameter) and the distributions measured by the APS (>0.54 µm in aerodynamic diameter), will not always provide a continuous distribution because the conversion from mobility to aerodynamic diameter is dependent upon the effective density. Based on the effective densities used for this study, we expect a gap between the size distributions measured by the EEPS and APS (Quiros et al. 2015a), and therefore the actual contribution for particles larger than a 560 nm mobility diameter can potentially be larger than the 4–23% reported in this study. Notwithstanding the trends shown here, the contribution of re-entrained or directly emitted coarse mode particles to total PM emissions deserves further evaluation for a larger sample of light-duty vehicles compliant to the LEV III standards operating under transient conditions. Meantime, there is a gap in measurement range (560–1700/1240 nm) in which the PM were not captured by either EEPS or APS and it could be a reason still for underestimating gravimetric mass by IPSD method.

4. Conclusions

This study used real-time size distribution measurements from the EEPS with two matrices (the Default Matrix and a new released matrix, the Soot Matrix) to estimate PM mass emission rates with the IPSD method (M_{IPSD}) and compares them with the standard filter-based gravimetric method (M_{Grav}). M_{IPSD} was also compared to the soot emission rates estimated by the AVL MSS, a photo-acoustic soot sensor (M_{Soot}). Twenty tests were conducted using 10 light-duty vehicles over the transient FTP cycle. Results

show moderate to strong correlations between the M_{IPSD} and M_{Grav} ($R^2 = 0.53\text{--}0.87$ without intercept and $0.67\text{--}0.90$ with intercepts) from tests conducted on GDI vehicles. Correlations were negative or insignificant from tests conducted on PFI or LDD vehicles. The Soot Matrix significantly improved the agreements between the M_{IPSD} and M_{Grav} with the GDI vehicle tests, by increasing the linear regression slopes from 0.58 to 1.02 and from 0.57 to 0.93 with two different filter setups. The improvements on PFI vehicles were about proportional to those on the GDI vehicles; however, mass estimated using IPSD was still 43–91% lower than the gravimetric reference method.

For all GDI, PFI, and LDD vehicles, strong correlations and one-to-one relationships were observed between M_{IPSD} and M_{Soot} , indicating the EEPS Soot Matrix is robust for predicting PM mass when the emissions are mostly comprised of solid soot particles. Additionally, the emission rates from PFI and LDD vehicles (below 1 mg/mile) were typically lower than GDI vehicles (greater than 1 mg/mile). Therefore, any fixed contribution of larger coarse-mode particles emitted from the engine or re-entrained from the sampling or semi-volatile contribution onto filter media would have composed a larger proportion of total PM mass. For example, an estimated 23% of the PFI emissions, and only 4–8% of the GDI emissions were beyond the EEPS measurement range as detected by the APS during select tests.

Acknowledgments

HJ and XW thank TSI for technical support and permission on use of the new Soot Matrix before its official release. The authors thank Mr. Kurt Bumiller for his contribution in conducting the emissions testing for this program. HJ is grateful to William Silvis for description of MSS calibration procedure.

Funding

This program was supported by the California Air Resources Board under contract 11-548.

ORCID

Heejung S. Jung  <http://orcid.org/0000-0003-0366-7284>

References

ARB (2015). An Update on the Measurement of PM Emission at LEV III Levels. Available at http://www.arb.ca.gov/msprog/levprog/leviii/lev_iii_pm_measurement_feasibility_tsd_20151008.pdf

Bahreini, R., Xue, J., Johnson, K., Durbin, T., Quiros, D., Hu, S., Huai, T., Ayala, A., and Jung, H. (2015). Characterizing

Emissions and Optical Properties of Particulate Matter from PFI and GDI Light-duty Gasoline Vehicles. *J. Aerosol Sci.*, 90:144–153.

Biskos, G., Reavell, K., and Collings, N. (2005). Description and Theoretical Analysis of a Differential Mobility Spectrometer. *Aerosol Sci. Technol.*, 39:527–541.

CFR (2011). Code of Federal Regulations, 40 Parts, PART 1065—ENGINE-TESTING PROCEDURES. Available at http://www.ecfr.gov/cgi-bin/text-idx?tpl=/ecfrbrowse/Title40/40cfr1065_main_02.tpl

CFR (2012). Code of Federal Regulations, 40 Parts, PART 1066—VEHICLE-TESTING PROCEDURES. Available at http://www.ecfr.gov/cgi-bin/text-idx?tpl=/ecfrbrowse/Title40/40cfr1066_main_02.tpl

Combustion (2007). Calibration of DMS Series Fast Particulate Spectrometers. Available at http://www.cambustion.com/sites/default/files/instruments/DMS500/dms_calibrationv3.pdf

Donaldson, K., Li, X. Y., and Macnee, W. (1998). Ultrafine (nanometre) Particle Mediated Lung Injury. *J. Aerosol Sci.*, 29:553–560.

EPA (2002). *Health Assessment Document for Diesel Engine Exhaust*. United States Environmental Protection Agency, EPA/600/8-90/057F. US EPA, Washington, DC. Available at <http://cfpub.epa.gov/ncea/cfm/recordisplay.cfm?deid=29060#Download>.

EPA (2015). AirData Download Files from EPA. Available at aqsdrl.epa.gov/aqswweb/aqstmp/airdata/download_files.html

Fujita, E. M., Zielinska, B., Campbell, D. E., Arnott, P., Sagebiel, J. C., Mazzoleni, Li, and Chow, J. C. (2007). Variations in Speciated Emissions from Spark-ignition and Compression-ignition Motor Vehicles in California's South Coast Air Basin. *Air Waste Manage. Assoc.*, 57:705–720.

Giechaskiel, B., Mamakos, A., Andersson, J., Dilara, P., Martini, G., Schindler, W., and Bergmann, A. (2012). Measurement of Automotive Nonvolatile Particle Number Emissions within the European Legislative Framework: A Review. *Aerosol Sci. Technol.*, 46:719–749.

Holm, R. L., Caldow, R., Hairston, P. P., Quant, F. R., and Sem, G. J. (1997). An Enhanced Time-of-Flight Spectrometer that Measures Aerodynamic Size Plus Light-Scattering Intensity. *J. Aerosol Sci.*, 28:S11–S12.

Hu, S. H., Zhang, S. Y., Sardar, S., Chen, S. Y., Dzhema, I., Huang, S. M., Quiros, D., Sun, H. W., Laroo, C., Sanchez, L. J., Watson, J., Chang, M. C. O., Huai, T., and Ayala, A. (2014). Evaluation of Gravimetric Method to Measure Light-Duty Vehicle Particulate Matter Emissions at Levels below One Milligram per Mile (1 mg/mile). *SAE Paper 2014-01-1571*:10.4271/2014-4201-1571.

Johnson, K. C., Xue, J., Russell, R. L., Durbin, T. D., Miller, W., and Jung, H. J. (2015). Final Report: Very low PM Mass Measurements. CRC Report No. E-99. Available at: <https://www.arb.ca.gov/research/apr/past/12-320.pdf>

Kamboures, M., Hu, S., Yu, Y., Sandoval, J., Rieger, P., Huang, S., Zhang, S., Dzhema, I., Huo, D., Ayala, A., and Chang, M. C. (2013). Black Carbon Emissions in Gasoline Vehicle Exhaust: A Measurement and Instrument Comparison. *Air Waste Manage. Assoc.*, 63:886–901.

Kamboures, M. A., Rieger, P. L., Zhang, S., Sardar, S. B., Chang, M. C. O., Huang, S. M., Dzhema, I., Fuentes, M., Benjamin, M., Hebert, A., and Ayala, A. (2015). Evaluation of a

- Method for Measuring Vehicular PM with a Composition Filter and a Real-time BC Instrument. *Atmos. Environ.*, 123:63–71.
- Kasper, M. (2009). CAST-Combustion Aerosol Standard: Principle and New Applications. Available at <http://www.sootgenerator.com/documents/Kasper.pdf>
- Kittelson, D. B. (1998). Engines and Nanoparticles: A Review. *J. Aerosol Sci.*, 29:575–588.
- Li, Y., Xue, J., Johnson, J. P., Durbin, T. D., Villeta, M., Pham, L., Hosseini, S., Zheng, Z., Short, D., Karavalakis, G., Awuku, A., Jung, H. J., Wang, X. L., Quiros, D., Hu, S. H., Huai, T., and Ayala, A. (2014). Determination of Suspended Exhaust PM Mass for Light-Duty Vehicles. *SAE Technical Paper 2014-01-1594*.
- Liu, Z. G., Vasys, V. N., Dettmann, M. E., Schauer, J. J., Kittelson, D. B., and Swanson, J. (2009). Comparison of Strategies for the Measurement of Mass Emissions from Diesel Engines Emitting Ultra-Low Levels of Particulate Matter. *Aerosol Sci. Technol.* 42:1142–1152.
- Maricq, M. M., Szente, J., Loos, M., and Vogt, R. (2011). Motor Vehicle PM Emissions Measurements at LEVIII Levels. *SAE Technical Paper 2011-01-0623*.
- Maricq, M. M., and Xu, N. (2004). The Effective Density and Fractal Dimension of Soot Particles from Premixed Flames and Motor Vehicle Exhaust. *J. Aerosol Sci.*, 35:1251–1274.
- Maricq, M. M., Szente, J. J., Harwell, A. L., and Loos, M. J. (2016). How Well can Aerosol Instruments Measure Particulate Mass and Solid Particle Number in Engine Exhaust? *Aerosol Sci. Technol.*, 50(6):605–614.
- Mirme, A. (1994). Electric Aerosol Spectrometry. Doctoral thesis, Tartu University, Tartu, Estonia.
- Mohr, M., Lehmann, U., Rutter, J. (2005). Comparison of Mass-Based and Non-Mass-Based Particle Measurement Systems for Ultra-Low Emissions from Automotive Sources. *Environ Sci Technol.*, 39(7): 2229–2238.
- Oberdorster, G., Sharp, Z., Atudorei, V., Elder, A., Gelein, R., Kreyling, W., and Cox, C. (2004). Translocation of Inhaled Ultrafine Particles to the Brain. *Inhalation Toxicol.*, 16:437–445.
- Peters, T. M., and Leith, D. (2003). Concentration Measurement and Counting Efficiency of the Aerodynamic Particle Sizer 3321. *J. Aerosol Sci.*, 34:627–634.
- Quiros, D. C., Hu, S. H., Hu, S. S., Lee, E. S., Sardar, S., Wang, X. L., Olfert, J. S., Jung, H. J. S., Zhu, Y. F., and Huai, T. (2015a). Particle Effective Density and Mass During Steady-State Operation of GDI, PFI, and Diesel Passenger Cars. *J. Aerosol Sci.*, 83:39–54.
- Quiros, D. C., Zhang, S., Sardar, S., Kamboures, M. A., Eiges, D., Zhang, M., Jung, H. S., Mccarthy, M. J., Chang, M. C. O., Ayala, A., Zhu, Y. F., Huai, T., and Hu, S. H. (2015b). Measuring Particulate Emissions of Light Duty Passenger Vehicles Using Integrated Particle Size Distribution (IPSD). *Environ. Sci. Technol.*, 49:5618–5627.
- Sardar, S., Zhang, S., Larsen, L., Frodin, B., McMahon, W., Huang, S. M., and Oliver, C. M. C. (2016). Evaluation of PM Measurement Precision and the Quivalency of the Single and Three Filter Sampling Methods for LEV III FTP Standards. *SAE Int. J. Engines.* 9:342–354. doi:10.4271/2015-01-9045
- Schindler, W., Haisch, C., Beck, H. A., Niessner, R., Jacob, E., and Rothe, D. (2004). A Photoacoustic Sensor System for the Time Resolved Quantification of Diesel Soot Emission. *SAE Technical Paper 2004-01-0969*.
- Symonds, J., and Reavell, K. (2007). Calibration of a Differential Mobility Spectrometer. *European Aerosol Conference, Salzburg*, 9–14 September, 2007. Available at <http://www.gaef.de/eac2007/eac2007abstracts/T02Abstractpdf/T02A034.pdf>
- Symonds, J., Reavell, K., Olfert, J., Campbell, B., and Swift, S. (2007). Diesel Soot Mass Calculation in Real-time with a Differential Mobility Spectrometer. *J. Aerosol Sci.*, 38:52–68.
- TSI (2015). Updated Inversion Matrices for Engine Exhaust Particle Sizer (EEPS) Spectrometer Model 3090. Available at http://tsi.com/uploadedFiles/_Site_Root/Products/Literature/Application_Notes/Updated_Inversion_Matrices_EEPS-005-A4-web.pdf
- Wang, X. L., Grose, M., Avenido, A., Stolzenburg, M. R., Caldow, R., Osmondson, B. L., Chow, J. C., and Watson, J. G. (2016a). Improvement of Engine Exhaust Particle Sizer (EEPS) Size Distribution Measurement - I. Algorithm and Applications to Compact Aerosols. *J. Aerosol Sci.*, 92:95–108.
- Wang, X. L., Grose, M., Caldow, R., Osmondson, B. L., Swanson, J., Chow, J. C., Watson, J. G., Kittelson, D. B., Li, Y., Xue, J., Jung, H. J., and Hu, S. H. (2016b). Improvement of Engine Exhaust Particle Sizer (EEPS) Size Distribution Measurement - II. Engine Exhaust Aerosols. *J. Aerosol Sci.*, 92:83–94.
- Xue, J., Li, Y., Wang, X. L., Durbin, T. D., Johnson, K. C., Karavalakis, G., Awuku, A., Villeta, M., Quiros, D., Hu, S. H., Huai, T., Ayala, A., and Jung, H. J. (2015). Comparison of Vehicle Exhaust Particle Size Distributions Measured by SMPS and EEPS During Steady-state Conditions. *Aerosol Sci. Technol.*, 49:984–996.
- Zheng, Z. Q., Durbin, T. D., Karavalakis, G., Johnson, K. C., Chaudhary, A., Cocker, D. R., Herner, J. D., Robertson, W. H., Huai, T., Ayala, A., Kittelson, D. B. and Jung, H. S. (2012). Nature of Sub-23-nm Particles Downstream of the European Particle Measurement Programme (PMP)-Compliant System: A Real-Time Data Perspective. *Aerosol Sci. Technol.*, 46:886–896.